

# Blue-sensitive organic photoconductive device with MDMO-PPV doped F8BT layer

Takeshi Fukuda, Sho Kimura, Zentaro Honda, and Norihiko Kamata

Department of Functional Materials Science, Saitama University

255 Shimo-Okubo, Sakura-ku, Saitama-shi, Saitama 338-8570, Japan

Corresponding author: Takeshi Fukuda

Electronic mail: fukuda@fms.saitama-u.ac.jp

Tel and Fax: +81-48-858-3526

By doping poly(9,9-dioctylfluorene-alt-benzothiadiazole) (F8BT) with poly(2-methoxy-5-(3'-7'-dimethyloctyloxy)-1,4-phenylenevinylene) (MDMO-PPV), improved photoconductive characteristics were obtained for an organic photoconductive device fabricated by a conventional spin-coating process. This device had a maximum external quantum efficiency (EQE) of 2.4% at 15 MV/m when the doping ratio of MDMO-PPV-doped F8BT was 50 wt%. This EQE is approximately 5.1 times higher than that (0.47%) of a reference device with undoped F8BT. In addition, the signal-to-noise ratio (i.e., photocurrent/dark current) was improved by doping MDMO-PPV because of the reduced dark current density. The highest signal-to-noise ratio obtained was 447.

Keyword: organic photoconductive device, color selectivity, solution process, fluorene polymer, organic image sensor, carrier dislocation

## Introduction

Since organic devices can be fabricated by a roll-to-roll printing process, many researchers have

investigated novel organic solution-processed devices such as light emitting diodes [1], photovoltaic cells [2], and transistors [3]. Several

printing methods have been investigated to further reduce fabrication costs and to achieve larger device areas than conventional Si-based semiconductor devices [4–9]. Several organic materials have selective absorption bands in the visible wavelength region [10–12] and color-sensitive organic image sensors have been fabricated by stacking several organic layers with different absorption bands [13]. The most significant advantage of organic materials over Si is that they have considerably higher absorption coefficients [11].

In single-layer devices, most photogenerated carriers recombine in the organic layer due to its short carrier diffusion length [14]. It is difficult to fabricate solution-processed multilayer devices. However, solution-processed single-layer devices have lower photoconductive characteristics than multilayer devices fabricated by a conventional thermal evaporation process [11, 15]. Doping techniques for have been widely investigated to realize a carrier dislocation structure in the organic layer of organic photovoltaic cells [5, 16, 17]. Our research group achieved enhanced photoconductive

characteristics by doping poly(dioctylfluorenyl-co-benzo-thiadiazole) (F8BT) with several silole derivatives [18, 19].

In the present study, we demonstrate improved photoconductive characteristics of a blue-sensitive organic device fabricated by a conventional spin-coating process. We used F8BT as a blue-sensitive polymer [11] and poly(2-methoxy-5-(3'-7'-dimethyloctyloxy)-1,4-phenylenevinylene) (MDMO-PPV) as a carrier dislocation element in F8BT. F8BT is a suitable photoconductive polymer for blue-sensitive devices as it has a high carrier mobility [20] and a strong absorption in the blue wavelength region [11]. We used it to fabricate a blue-sensitive organic sensor in a previous study [12].

## **Experimental**

A glass substrate coated with patterned indium tin oxide (ITO) was ultrasonically cleaned with organic solvents and deionized water. The ITO-coated glass substrate was then treated with ultraviolet ozone for 20 min. A 150-nm-thick ITO layer was deposited by a conventional sputtering method. A blue-sensitive organic photoconductive

polymer F8BT (American Dye Source, Inc.) (1 wt%) was dissolved in chloroform. MDMO-PPV (Aldrich) was added to the resulting solution. We varied the doping concentration of MDMO-PPV in F8BT in the range 0 to 50 wt% to determine the concentration dependence of the photoconductive characteristics of organic photoconductive devices. Figure 1 shows a cross-sectional view of the fabricated organic photoconductive device and the molecular structures of F8BT and MDMO-PPV, which were used in the photoconductive layer of the device.

After passing through a filter with 0.45- $\mu\text{m}$ -diameter holes, the organic solution was spin coated at a rotational speed of 2000 rpm for 60 s in a nitrogen atmosphere. The sample was then annealed at 70 °C for 60 min to remove any residual chloroform. Finally, LiF (1 nm) and Al (100 nm) layers were thermally evaporated successively on the MDMO-PPV:F8BT layer.

The external quantum efficiency (EQE), defined as the ratio of the number of output electrons to the total number of irradiated photons, was estimated from the measured photocurrent and the irradiated

light intensity [11]. We used a blue light-emitting diode (LED) with wavelength of 470 nm. The blue light intensity was 1 mW/cm<sup>2</sup> and the focus area was almost the same as the device area. The photocurrent was measured while irradiating the blue light and the dark current was measured without the blue light. In addition, the signal-to-noise ratio (S/N) was estimated by dividing the photocurrent density by the dark current density.

## Results and Discussion

The measured thicknesses of the organic layers were 210 nm (0 wt%), 210 nm (10 wt%), 170 nm (20 wt%), 270 nm (30 wt%), 320 nm (40 wt%), and 1100 nm (50 wt%). The thickness increased with increasing MDMO-PPV concentration.

Figure 2(a) shows the effect of the applied electric field on the photocurrent density when the device was irradiated by 1 mW/cm<sup>2</sup> of blue light. The electric field was calculated by dividing the applied voltage by the thickness of the MDMO-PPV-doped-F8BT layer. The photocurrent density initially decreased drastically with increasing MDMO-PPV doping concentration. It subsequently increased with increasing MDMO-PPV doping

concentration up to 50 wt%. This indicates that MDMO-PPV suppresses carrier transport in the organic layer. The absorption coefficient of F8BT is  $138,000 \text{ cm}^{-1}$  at 470 nm [11], which is much higher than that of MDMO-PPV. Consequently, carriers are generated in F8BT when the organic photoconductive device is irradiated by blue light. The carriers move toward the electrode when a bias voltage is applied.

Figure 2(b) shows the relationship between the applied electric field and the dark current density. The dark current density was relatively unaffected by the MDMO-PPV concentration. Since the noise level in our experimental setup was less than  $10 \text{ nA/cm}^2$ , we could not precisely determine the effect of the doping concentration on the dark current density. However, a low dark current density was realized at all MDMO-PPV concentrations, which indicates that MDMO-PPV doping may be suitable for blue-sensitive organic photoconductive device.

To investigate carrier transport in MDMO-PPV-doped F8BT, the energy diagram of the fabricated organic photoconductive device is shown in Fig. 3. Since MDMO-PPV is an electron acceptor due its

low ionization potential (5.3 eV) [21], photogenerated electrons move from the lowest unoccupied molecular orbital (LUMO) level of F8BT to that of MDMO-PPV. The LUMO level of MDMO-PPV is 2.8 eV; therefore, the difference between the LUMO level of the organic layer and the ionization potential of the electrode is 1.9 eV for ITO and 1.5 eV for Al. The energy barrier at the electrode/organic interface is 1.1 eV on the ITO electrode side and 0.7 eV on the Al electrode side with no MDMO-PPV doping. This indicates that MDMO-PPV doping reduces the efficiency of electron transport from the organic layer to the electrode. Consequently, the photocurrent density decreased on doping F8BT with MDMO-PPV, as shown in Fig. 2(a).

In addition, since MDMO-PPV has a lower ionization potential than F8BT, MDMO-PPV and F8BT act as electron acceptors and donors, respectively. As a result, photogenerated carriers are efficiently dislocated in the MDMO-PPV-doped F8BT layer because of the large ionization potential difference. The dislocated carriers are efficiently transported from the F8BT to the electrode with a

low recombination probability. Therefore, the photocurrent density increased with increasing MDMO-PPV concentration, as shown in Fig. 2(a). The highest occupied molecular orbital level of MDMO-PPV is 5.3 eV, which is intermediate between that of F8BT (6.0 eV) and the ionization potential of the ITO (4.7 eV)/Al (4.3 eV) electrode. Therefore, the photogenerated holes efficiently move to the electrode side when a positive or negative bias voltage is applied.

Figure 4(a) shows the influence of the applied electric field on the EQE of the organic photoconductive device, which was calculated from the photocurrent density shown in Fig. 2(a). The relationship between the EQE and the electric field exhibits the same trend as the photocurrent density. The EQE initially decreased drastically on MDMO-PPV doping and then increased with increasing MDMO-PPV concentration up to 50 wt%. This result can be explained by the increased photocurrent density. In other words, the increased photocurrent density increases the EQE because the EQE is directly proportional to the photocurrent density [11]. Doping F8BT with MDMO-PPV is an

effective way of increasing the EQE.

Figure 4(b) shows the EQE of a fabricated device as a function of the electric field. The EQE continually increases with increasing electric field strength for all concentrations. This is because the carrier mobility of organic materials tends to increase with increasing electric field strength [22]. Therefore, the photogenerated carriers efficiently move to the electrode with a low carrier recombination probability, resulting in a high EQE.

Figure 5 shows the relationship between the electric field strength and the S/N of organic photoconductive devices with different MDMO-PPV doping concentrations. The devices with the two lowest doping concentrations (10 and 20 wt%) have lower S/Ns than the reference device that did not have MDMO-PPV doping. On the other hand, the S/N increased with increasing photocurrent density with increasing doping concentration (Fig. 2(a)). The S/N of the reference sample was 6 at 8.7 MV/m. In contrast, the maximum S/N (447) was obtained by the device with a concentration of 50 wt% at the same electric field; this S/N is approximately 75 times higher than that of the

reference device.

## Conclusion

We increased the EQE of a photoconductive device by doping F8BT with MDMO-PPV. A maximum EQE of 2.4% was realized at a MDMO-PPV concentration of 50 wt% at 15 MV/m. The energy diagram predicts that doping with MDMO-PPV should give a lower EQE; however, the carrier dislocation efficiency is considered to increase with increasing MDMO-PPV concentration because of the large ionization potential difference between MDMO-PPV and F8BT. The S/N also drastically increased with increasing MDMO-PPV concentration; a maximum S/N of 447 was achieved. These results indicate the potential of fabricating a high-performance organic image sensor by a solution process.

The maximum EQE of 2.4% is too low for practical applications; however, our experimental result demonstrates that MDMO-PPV doping is an effective technique for improving device performance.

## References

[1] Burroughes, J.H., Bradley, D.D.C., Brown A.R.,

Marks, N., Mackay, K., Fried, R.H., Burns, P.L., & Holmes, A.B., (1990). *Nature*, 347, 539.

[2] Smilowitz, L., Sariciftci, N.S., Wu, R., Gettinger, C., Heeger, A.J., & Wudl, F., (1993). *Phys. Rev. B*, 47, 13835.

[3] Meijer, E.J., Leeuw, D.M.de, Setayesh, S., Veenendaal, E.van, Huisman, B.-H., Blom, P.W.M., Hummelen, C., Scherf, U., & Klapwijk, T.M., (2003). *Nature Mater.*, 2, 678.

[4] Krebs, F.C., (2009). *Sol. Ener. Mater. Sol. Cells*, 93, 394.

[5] Blankenburg, L., Schultheis, K., Schache, H., Sensfuss, S., & Schrödner, M., (2009). *Sol. Ener. Mater. Sol. Cells*, 93, 476.

[6] Mori, K., Ning, T., Ichikawa, M., Koyama, T., & Taniguchi, Y., (2001). *Jpn. J. Appl Phys.*, 39, L942.

[7] Bassani, D.M., Junusauskaite, L., Cambot, A.L.-, McClenaghan, N.D., Pozzo, J.-L., Ray, D., & Vives, G., (2010). *Coord. Chem. Rev.*, 254, 2429.

[8] Ju, J., Yamagata, Y., & Higuchi, T., (2009). *Adv. Mater.*, 21, 1.

[9] Fukuda, T., Suzuki, T., Kobayashi, R., Honda, Z., & Kamata, N., (2009). *Thin Solid Films*, 518,

- 575.
- [10] Lamprecht, B., Thünauer, R., Köstler, S., Jakopic, G., Leising, G., & Krenn, J.R., (2008). *Phys. Stat. Sol. (RRL)*, 2, 178.
- [11] Fukuda, T., Komoriya, M., Kobayashi, R., Ishimaru, Y., & Kamata, N., (2009). *Jpn. J. Appl. Phys.*, 47, 04C162.
- [12] Fukuda, T., Komoriya, M., Mori, R., Honda, Z., Takahashi, K., & Kamata, N., (2009). *Mol. Cryst. Liq. Cryst.*, 504, 212.
- [13] Aihara, S., Seo, H., Namba, M., Watabe, T., Ohtake, H., Kubota, M., Egami, N., Hiramatsu, T., Matsuda, T., Furuta, M., Nitta, H., & Hirao, T., (2009). *IEEE Trans. Electron. Dev.*, 56, 2570.
- [14] Toušek, J., Toušková, J., Křivka, I., Pavlačková, P., Výprachtický, D., & Cimrova, V., (2010). *Org. Electron.*, 11, 50.
- [15] Aihara, S., Miyakawa, K., Ohkawa, Y., Matsubara, T., Takahata, T., Suzuki, S., Kubota, M., Tanioka, K., Kamata, N., & Terunuma D., (2005). *Jpn. J. Appl. Phys.*, 44, 3743.
- [16] Nelson, J., (2002). *Org. Electron.*, 6, 87.
- [17] Pivrikaas, A., Sariciftci, N.S., Juška, G., & Österbacka, R., (2007). *Prog. Photovolt: Res. Appl.*, 15, 677.
- [18] Kobayashi, R., Fukuda, T., Suzuki, Y., Hatano, K., Kamata, N., Aihara, S., Seo, H., & Terunuma, D., (2010). *Mol. Cryst. Liq. Cryst.*, 519, 206.
- [19] Fukuda, T., Kobayashi, R., Kamata, N., Aihara, S., Seo, H., Hatano, K., & Terunuma, D., (2010). *Jpn. J. Appl. Phys.*, 49, 01AC05.
- [20] Chua, L.-L., Zaumeil, J., Chang, J.-F., Ou, E. C.-W., Ho, P.K.-H., Siringhaus, H., & Friend, R.H., (2005). *Nature*, 434, 194.
- [21] Al-Ibrahim, M., Konkin, A., Roth, H.-K., Egbe, D.A.M., Klemm, E., Zhokhavets, U., Gobsch, G., & Sensfuss, S., (2005). *Thin Solid Films*, 474, 201.
- [22] Kim, Y., Cook, S., Choulis, A., Nelson, J., Durrant, J.R., & Bradley, D.C., (2004). *Chem. Mater.*, 16, 4812.

## Figure Captions

Fig. 1 Cross-sectional view of organic photoconductive device and molecular structures of F8BT and MDMO-PPV, which were used as photoconductive materials.

Fig. 2 (a) Photocurrent density and (b) dark current density as a function of applied electric field. MDMO-PPV concentrations of 0, 10, 20, 30, 40, and 50 wt% were used. A blue light intensity of  $1 \text{ mW/cm}^2$  was used to measure the photocurrent density.

Fig. 3 Energy diagram of fabricated organic photoconductive device with MDMO-PPV-doped F8BT as the photoconductive layer.

Fig. 4 (a) EQE of devices with different MDMO-PPV concentrations as a function of the applied electric field. (b) Relationship between applied electric field and the EQE for a positive bias voltage. MDMO-PPV concentrations of 0, 10, 20, 30, 40, 50 wt% were used to determine the optimal concentration.

Fig. 5 S/N of organic photoconductive device for various MDMO-PPV concentrations. S/N was calculated by dividing the photocurrent density by the dark current density.

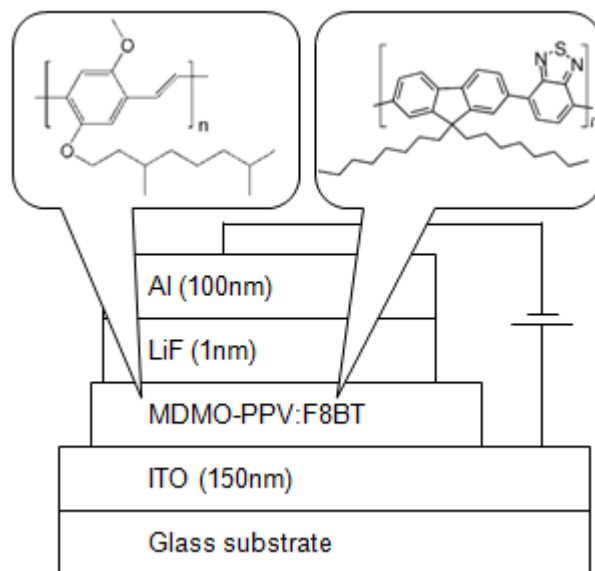


Fig. 1. Cross sectional view of organic photoconductive device and molecular structures of F8BT and MDMO-PPV used as photoconductive materials.

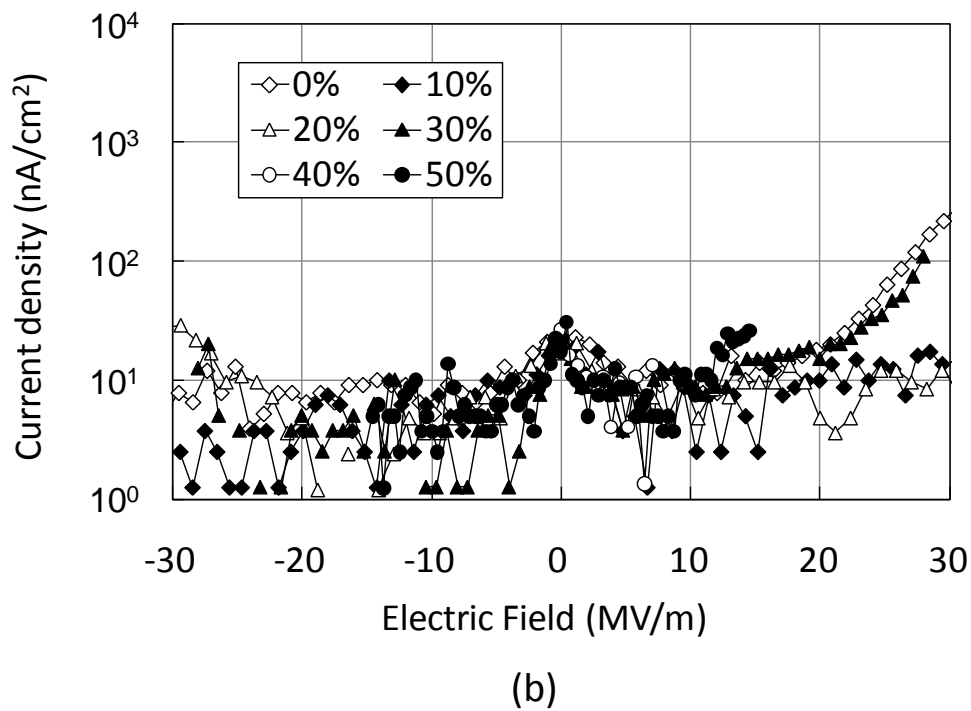
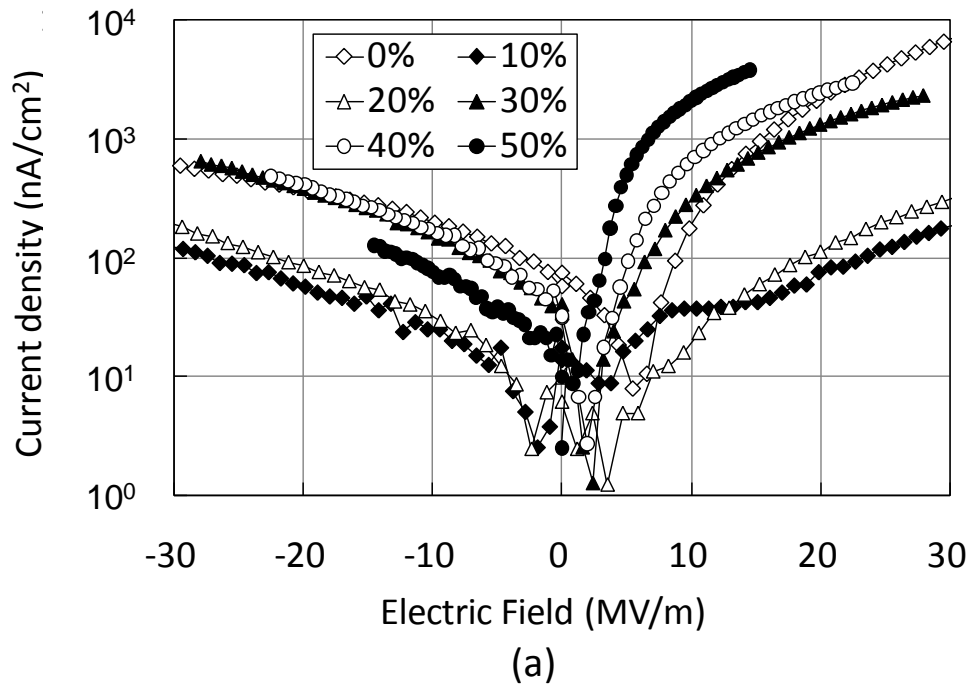


Fig. 2. (a) Photocurrent density and (b) dark current density as a function of applied electric field. MDMO-PPV concentrations of 0, 10, 20, 30, 40, and 50 wt% were used. A blue light intensity of  $1 \text{ mW/cm}^2$  was used to measure the photocurrent density.

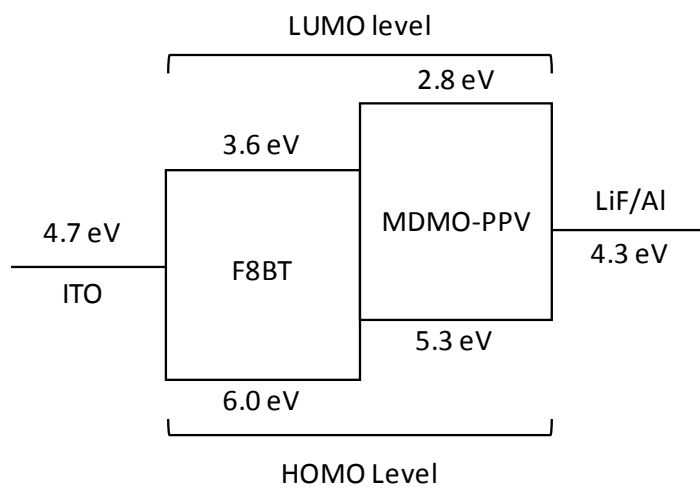
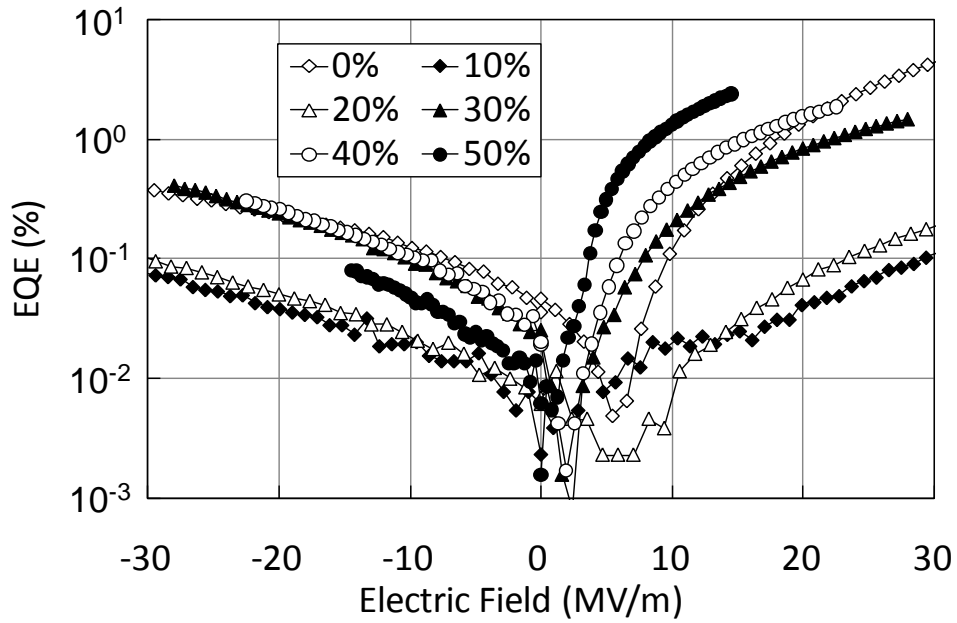
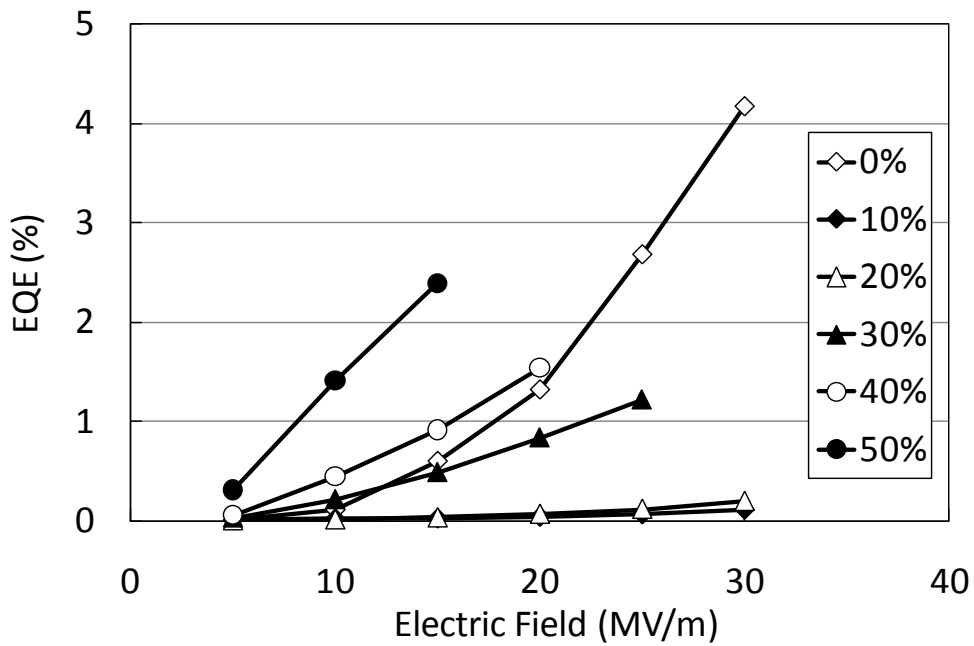


Fig. 3 Energy diagram of fabricated organic photoconductive device with MDMO-PPV-doped F8BT as the photoconductive layer.



(a)



(b)

Fig. 4. (a) EQE of devices with different MDMO-PPV concentrations as a function of the applied electric field. (b) Relationship between applied electric field and the EQE for a positive bias voltage. MDMO-PPV concentrations of 0, 10, 20, 30, 40, 50 wt% were used to determine the optimal concentration.

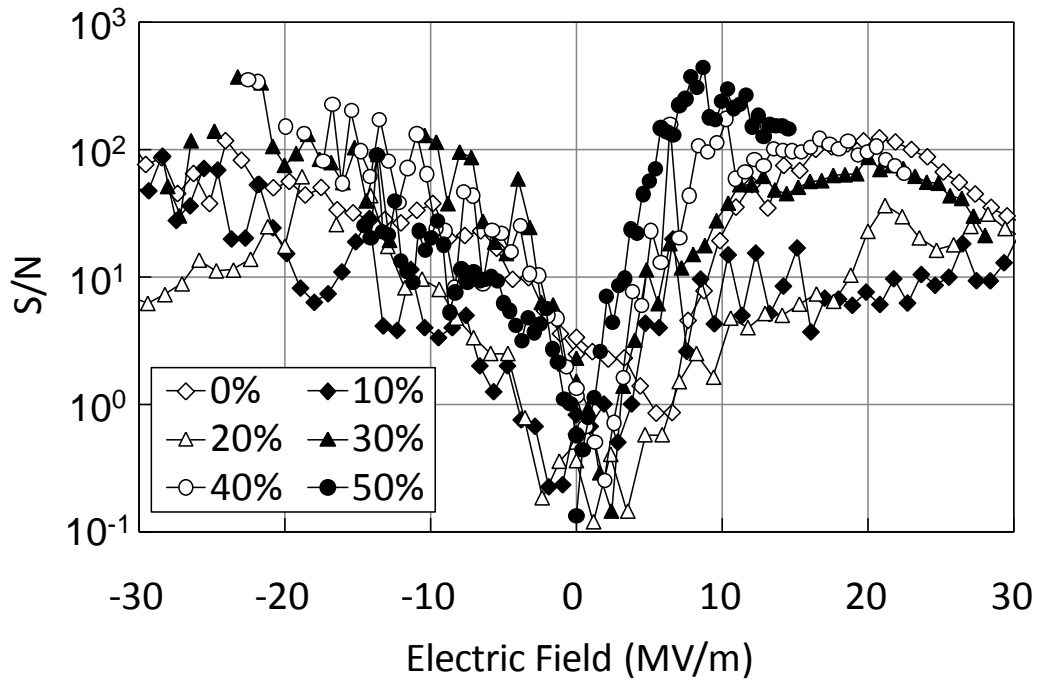


Fig. 5. S/N of organic photoconductive device for various MDMO-PPV concentrations. S/N was calculated by dividing the photocurrent density by the dark current density.